J Electroceram (2007) 19:147–164
DOI 10.1007/s10832-007-9042-5

# Recent advancements in magnetoelectric particulate and laminate composites

**Shashank Priya · Rashed Islam · Shuxiang Dong · D. Viehland**

Received: 31 May 2006 / Accepted: 20 September 2006 / Published online: 28 February 2007


**Abstract** Recently, the magnetoelectric (ME) effect—dielectric polarization of a material under magnetic field, or induced magnetization under an electric field—has become the focus of significant research interests. The primary requirement for the observance of said effect is the coexistence of magnetic and electric dipoles. Most of the known single phase materials suffer from the drawback that the ME effect is quite small, even at low temperatures limiting their applicability in practical devices. Better alternatives are ME composites, which have large magnitudes of the ME voltage coefficient. Composites exploit the product property of materials; where the ME effect is realized by combining magnetostrictive and piezoelectric phases that independently are not ME, but acting together (i.e., their product) result in a ME effect. In this review article, we survey recently reported results concerning ME composites, focusing on ME particulate (synthesized via a controlled precipitation technique) and laminated composites. The article also provides a survey of the compositions and magnitudes of the ME coefficients reported in the literature; a brief description of the analytical models developed to explain and predict the behavior of composites; and discuss several applications that are made possible by enhanced ME effects.

S. Priya (✉) · R. Islam
Automation and Robotics Research Institute, Materials Science and Engineering, The University of Texas, Arlington, TX 76019, USA
e-mail: spriya@uta.edu

S. Dong · D. Viehland
Materials Science and Engineering, Virginia Tech, Blacksburg, VA, USA

**Keywords** Magentoelectric · Ferroelectric · Magnetostrictive · Piezoelectric · Sensor · Energy harvesting · Phase shifter · Transformer

## 1 Introduction

Magnetoelectric (ME) materials become magnetized when placed in an electric field, and/or electrically polarized when placed in a magnetic field. Dielectric polarization of a material under the magnetic field or an induced magnetization under an electric field requires the simultaneous presence of long-range ordering of magnetic moments and electric dipoles. The conditions for the occurrence of ferroelectricity and magnetic order in the same material, often accompanied by ferroelasticity, implies (a) the presence of adequate structural building blocks permitting ferroelectric-type ionic movements, (b) magnetic-interaction pathways, usually of the superexchange type, and (c) the fulfillment of symmetry conditions [1]. One simple inference is that it should be possible to synthesize ferroelectric-ferromagnets (i.e., ferroelectromagnets) by replacing diamagnetic ions with paramagnetic ones: for example, on the B-site of oxygen octahedral ferroelectric perovskites. Smolensky and Ioffe [2] were the first to try said approach, nearly a half century ago, in the antiferromagnetic-ferroelectric perovskite $Pb(Fe_{1/2}Nb_{1/2})O_3$ (or PFN). Confirmation of a weak spontaneous magnetic moment in the ferroelectric phase below 9 K was later confirmed [3].

Recently, magnetoelectric materials have attracted significant attention from the scientific community as evidenced by the rising number of publications in the last 5 years. Figure 1 shows the results of a simple search on the INSPEC database using the two key words together "magnetoelectric" and "piezoelectric." The results of this

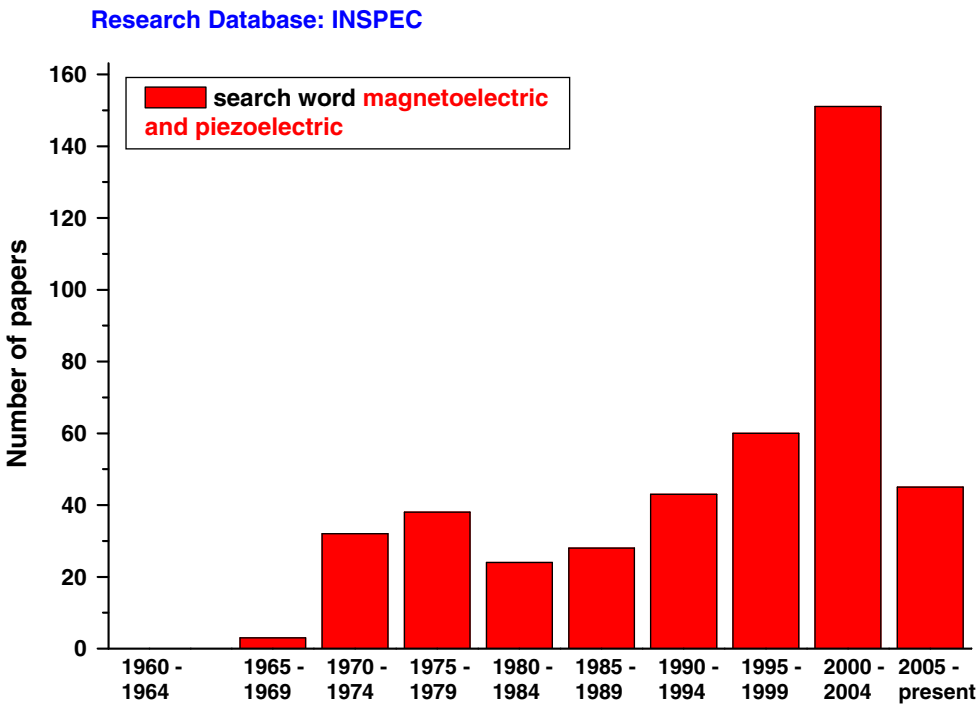


**Fig. 1** Search results on the INSPEC database using the two key words together "magneto-electric" and "piezoelectric"

search clearly highlight the revival of interest in this phenomenon. Materials exhibiting the ME effect can be classified in two classes: single phase and composites. Single phase materials exhibiting ME effects should show two coupled-transitions: one from ferroelectric to para-electric states, and another from ferro/ferri/antiferro-magnetic to paramagnetic states: the ME effect then arises due to coupling between the magnetic and polar sublattices. Recent investigations of single phase multiferroics have revealed that the origin of the ME effect is often associated with a particular exchange mechanism for various families of compounds, as listed in Table 1. [4–13] Orbital ordering, Jahn–Teller distortion, super/double exchange, and/or geometric magnetic frustration have been cited as the origin source of ME effects. An excellent review on this subject can be found in reference [12].

Suryanarayana has reviewed the ME effect for the family of compounds represented by the general formula $Bi_4Bi_{m-3}Ti_3Fe_{m-3}O_{3m+3}$, where compounds with $m$=4, 5, 6, 7 and 8 have been successfully synthesized [14, 15]. The maximum magnitude of the ME coefficient for $Bi_5FeTi_3O_{15}$ was found to be 17 mV/cm·Oe under a DC bias of 8,000 Oe; while for $Bi_6Fe_2Ti_3O_{12}$, it was 3.2 mV/cm·Oe under 4,000 Oe [14, 16]. Recent investigations of $Bi_8Fe_4Ti_3O_{24}$ have reported a ME coefficient of 0.35 mV/cm·Oe at room temperature [17]. In general, it has been found that as the Fe content increases in these compounds that the magnitude of the ME coefficient decreases.

Recently, the ferromagnetoelectric material $BiFeO_3$ has been investigated in thin film form [18, 19]. First, it is relevant to mention that $BiFeO_3$-based bulk materials have previously been reported to exhibit extremely small ferroelectric polarization and ferromagnetic magnetization: which might possibly be due to low resistivities and high coercive fields in crystals and ceramics. The magnitude of the ME coefficient of bulk materials has been reported to be on the order of 0.064 mV/cm·Oe under a magnetic bias of 9,500 Oe [14]. However, epitaxial thin-films of $BiFeO_3$ grown on $(001)_c$ $SrTiO_3$ [20] have been found to exhibit large ferroelectric responses. The saturation polarization $P_s$

**Table 1** Magnetoelectric effect in single phase materials.

| Compound | Mechanism |
|---|---|
| $BiFeO_3$, $BiMnO_3$ | Stereochemical activity of Bi lone pair |
| $YMnO_3$ | Buckling of the layered $MnO_5$ polyhedra, accompanied by displacements of the Y ions. |
| $TbMnO_3$, $DyMnO_3$, $TbMn_2O_5$ | Frustated spin resulting in magnetoelastically induced lattice modulations |
| $La_{0.5}Ca_{0.5}MnO_3$ | Charge ordering in doped perovskite structure |
| $CdCr_2S_4$ | Electronic super-exchange and soft mode behavior |

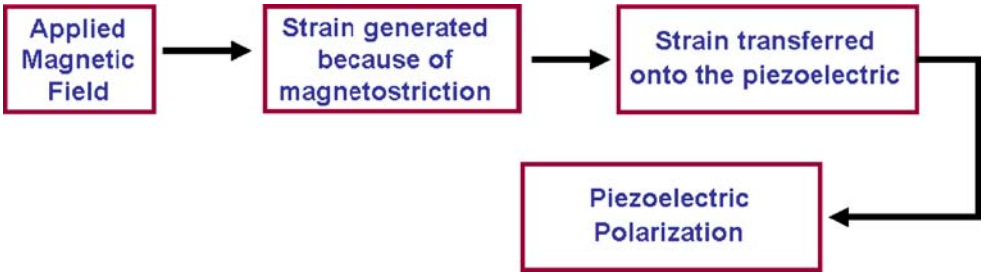


**Fig. 2** Schematic representation of the ME effect in the composites utilizing the product property [48]

of $(001)_c$ $BiFeO_3$ thin films has been reported to be ~0.6 C/m$^2$—which is ~20× larger than that of a bulk crystal projected onto the same orientation. Remanent polarizations $P_r$ of ~55 μC/cm$^2$ for $(001)_c$ films, ~80 μC/cm$^2$ for $(110)_c$ films, and ~100 μC/cm$^2$ for $(111)_c$ films have been reported [21]. The magnetization of the films at low magnetic field levels is dramatically increased, relative to that of bulk crystals. In the case of a $(111)_c$ film, the induced magnetization is on the order of 0.6 emu/g at $H_{ac}$=1 T, which is about an order of magnitude higher than that of bulk crystals under the same field.

Interestingly, several simple architecturally-engineered nano-structured $BiFeO_3$ materials have also recently been reported. First, by varying the oxygen pressure during deposition, the dominant phase in a $BiFeO_3$ film has been shown to continuously change from $BiFeO_3$ to a mixture of $\alpha$-$Fe_2O_3$ and $\gamma$-$Fe_2O_3$. This represents a new type of multiferroic: a nano-composite, where $\alpha$-$Fe_2O_3$ and $\gamma$-$Fe_2O_3$ are magnetostrictive and $BiFeO_3$ piezoelectric [22]. Second, the synthesis and characterization of ordered multiferroic $BiFeO_3$ nanotube arrays has also been reported [23]. Nanotubes with diameters of about 250 nm, wall thickness of 20 nm, and lengths of about 6 μm were fabricated using sol-gel method utilizing nano-channel alumina templates. Investigations have shown that $BiFeO_3$ maintains its ferroelectric properties in this morphological form: however, investigations have yet to be performed to exploit this architecture, and characterize its structure-property relations. This brings us to focus on the main topic of this review article that of piezoelectric-magnetostrictive ME particulate and laminate composites.

Unfortunately, single phase materials suffer from the drawback that the ME effect is extremely small at room temperature. For example, the highest ME coefficient has been reported for antiferromagnetic $Cr_2O_3$ crystals, which is $2.67\times10^{-12}$ s/m at a Neel temperature of 34 °C.

**Table 2** List of magnetoelectric composites reported in literature.

| Composition | Synthesis technique | Experimental conditions | DC Bias/Frequency | dE/dH (mV/cm·Oe) |
|---|---|---|---|---|
| 0.62 $BaTiO_3$–0.38 $CoFe_2O_4$ (eutectic composition with 1.5 wt% excess $TiO_2$) | Unidirectional solidification | Bridgman/1 atm $O_2$/50 cm h$^{-1}$ | ? | 50[24] |
| 0.60 $BaTiO_3$–0.40 $Ni_{0.97}Co_{0.03}Mn_{0.1}Fe_{1.90}O_4$ | Particulate | Sintered at 1,300 °C/24 h | 500 Oe/1 kHz | 80[25] |
| $CoFe_2O_4$–$Bi_4Ti_3O_{12}$ | Particulate | Sintered | ? | 0.12[14] |
| 0.3 $CuFe_2O_4$–0.7 $PbZr_{0.53}Ti_{0.47}O_3$ | Particulate | Sintered at 950 °C/2 h | 460 Oe/100 kHz | 421[26] |
| $Ni_{0.8}Zn_{0.2}Fe_2O_4$–0.41 vol% PZT | Particulate | Hot Pressed at 1,000 °C/7 Mpa | 250 Oe/100 Hz | 45[27] (transverse coefficient) |
| $Ni_{0.8}Zn_{0.2}Fe_2O_4$–0.75 vol% PZT | Particulate | Hot Pressed at 1,000 °C/7 Mpa | >1,000 Oe/270 kHz (*resonance effect*) | 3,300[27] |
| BaO–$TiO_2$–CoO–FeO solution | Particulate | Sintered in range of 1,000–1,200 °C/3 h | 30 Oe/1,070 Hz | 5.58[28] |
| $Bi_8Fe_4Ti_3O_4$ | Single phase | Sintering | 4,500 (f=?) | 0.35[29] |
| PZT–20 wt% $NiCo_{0.02}Cu_{0.02}Mn_{0.1}Fe_{1.8}O_4$ | Particulate | Sintered at 1,250 °C | 1,250 Oe/1 kHz | 115[30] |
| 0.75 $BaTiO_3$–0.25 $CuFe_2O_4$ | Particulate | Sintered at 1,200 °C/12 h | 1,000 Oe/DC | ~0.520[31] |
| 0.45 $CuFe_{1.6}Cr_{0.4}O_4$–0.55 $BaTiO_3$ | Particulate | Sintered at 1,100 °C/24 h | 1,570 Oe/DC | 0.0956[32] |
| Terfenol-D / $Pb(Mg_{1/3}Nb_{2/3})O_3$–$PbTiO_3$ / Terfenol-D | Laminate | Bonded using the silver epoxy/annealing at 80 °C | 4,000 Oe/1 kHz | 5,150[33](peak) |
| $NiFe_2O_4$–PZT | Multilayer | 11 layers of 13 μm $NiFe_2O_4$ 1 and 10 layers of 26 μm PZT | 1,050 Oe/350 kHz (resonance effect) | 1,200[34] |

**Table 3** Saturation magnetostriction of some representative magnetic materials at room temperature.

| Material | $\frac{3}{2}\lambda_s(\chi 10^{-6})$ | $T_c$ (°C) |
|---|---|---|
| Fe | −14 | 770 |
| Ni | −50 | 358 |
| Co | −93 | 1120 |
| 50% Co–50% Fe | 87 | 500 |
| 50% Ni–50% Fe | 19 | 500 |
| $TbFe_2$ | 2,630 | 423 |
| Tb | 3,000 (−196 °C) | −48 |
| Dy | 6,000 (−196 °C) | −184 |
| Terfenol-D | 1,620 | 380 |
| $Tb_{0.6}Dy_{0.4}$ | 6,000 (−196 °C) | ? |
| Metglas 2605SC | 60 | 370 |

For Tb, Dy and $Tb_{0.6}Dy_{0.4}$ the constants are reported at −196 °C.

However, composite materials are known to have significantly larger ME coefficients, as originally reported by Van Suchtelen [1]. A suitable combination of magnetostrictive and piezoelectric phases can yield dramatically enhanced ME effects, relative to single phase materials. Magnetoelastic interactions are known to be high in only a few magnetostrictive materials: accordingly, investigations of ME composites have focused on magnetostrictive layers, rather than peizomagnetic ones. In magnetostrictive materials, the strain induced by applied magnetic field is proportional to square of the magnetic field. An effective linear operational range can be achieved by applying a DC magnetic bias across the structure; i.e., by DC biasing the magnetostrictive layer to an effective piezomagnetic state. Figure 2 shows the schematic representation of the ME effect in the composites utilizing the product property. Table 2 lists some of the composite materials reported in literature, their magnitude and experimental conditions. [14, 24–34] It can be seen from this table that at low frequencies the magnitude of the ME effect can be as large as 115 mV/cm·Oe: which is ~300 times higher than that of $Cr_2O_3$.

Tables 3, 4 and 5 provide a list of magnetostrictive and piezoelectric materials of interest. [35–40] The properties listed include saturation magnetostriction $\lambda_s$, Curie temperature $T_c$, longitudinal piezoelectric strain constant $d_{33}$, transverse piezoelectric strain constant $d_{31}$, relative dielectric constant $\varepsilon_r$, and longitudinal coupling factor $k_{33}$. High magnetostrictive coefficients are obtained in the compounds of the type R-T where R is rare earth and T is the transition metal. Highly magnetostrictive rare earths (namely Sm, Tb, and Dy) have been combined with the magnetic transition metals Ni, Co, and Fe to obtain high induced strains at room temperature. An unusual behavior is found in case of R-Fe compounds, which exhibited an increase in the Curie temperature with increasing rare earth concentration. This abnormality facilitates a huge room temperature magnetostriction of up to $300\times10^{-6}$ in $TbFe_2$ at saturation fields of 2 MA/m. It has been found that partial substitution of Dy for Tb in the $TbFe_2$ results in giant enhancement of the magnetostrictive and anisotropy properties at low magnetic fields. The binary compound $Tb_{0.3}Dy_{0.7}Fe_{1.9-1.95}$ commercially known as Terfenol-D has the highest room-temperature magnetostriction of $1{,}600\times10^{-6}$ at a moderate saturation field of 0.16 MA/m. Terfenol-D is widely employed as the magnetostrictive material of choice in several important applications including active noise and vibration control systems, low frequency underwater communications (sonar), linear and rotational motors, and ultrasonic cleaning. This material also has importance as the magnetostrictive phase in ME laminate composites, as described later in this review.

The choice for the piezoelectric material in magnetoelectric composites is diverse including ceramics, single crystals, and polymers as shown in Table 5. [41–44] Selection depends on the fabrication technique used to synthesize the composite: such as mixed oxide ceramic processing, hot-pressing, lamination, high vacuum impregnation, co-firing, injection molding, and/or extrusion. The compound $Pb(Zr_xTi_{1-x})O_3$ (PZT) is commonly used as the piezoelectric material due to ease in processing, availability, and low costs. The material constants listed in Table 5 clearly indicate that the relaxor-ferroelectric single crystal might provide considerably higher performance, as compared to other piezoelectric materials. The drawbacks of the single crystals are low transition temperatures, higher nonlinearity, and larger temperature and vibration sensitivities.

## 2 Symmetry requirements for composites

The importance of symmetry in the design of magnetoelectric composites has been discussed in detail by several researchers. [45–47] The induced magnetization $B_i$ (axial first rank tensor) is proportional to the applied electric field $E_j$ (polar first rank tensor) through the magnetoelectric susceptibility

**Table 4** Saturation magnetostriction of some representative magnetic oxides at 20 °C.

| Material | $\lambda s$ ($\times 10^{-6}$) |
|---|---|
| $MnFe_2O_4$ | −5 |
| $Fe_3O_4$ | 40 |
| $CoFe_2O_4$ | −110 |
| $MgFe_2O_4$ | −6 |
| $Li_{0.5}Fe_{2.5}O_4$ | −8 |
| $NiFe_2O_4$ | −26 |
| $CuFe_2O_4$ | −9 |
| $YFe_5O_{12}$ | −2 |
| $SmFe_5O_{12}$ | 3.3 |
| $DyFe_5O_{12}$ | 1.46 |
| $EuFe_5O_{12}$ | 9.48 |

**Table 5** Dielectric and piezoelectric properties of some important piezoelectric materials.

| Material | $d_{33}$ (pC/N) | $d_{31}$ (pC/N) | $\varepsilon r$ (@ 1 kHz) | $k_{33}$ | $T_c$ (°C) |
|---|---|---|---|---|---|
| $BaTiO_3$ | 190 | −78 | 1,700 | 0.49 | 120 |
| APC 850 (soft PZT) | 400 | −175 | 1,750 | 0.72 | 360 |
| APC 855 (soft PZT) | 630 | −276 | 3,300 | 0.76 | 250 |
| APC 840 (hard PZT) | 290 | −125 | 1,250 | 0.72 | 325 |
| PZT–$Pb(Ni_{1/3}Nb_{2/3})O_3$ | 600 | −250 | 3,900 | 0.69 | 205 |
| <001>0.92 $Pb(Zn_{1/3}Nb_{2/3})O_3$–0.08 $PbTiO_3$ | 2,230 | −1,080 | 8,260 $\left(\varepsilon_{33}^{T}\right)$ | 0.94 | 170 |
| PVDF | | −28 | 6 | 0.2 ($k_t$) | 170 (melting temperature) |
| $SrBi_4Ti_4O_{15}$ | 20 | −3 | 150 | 0.2 | 550 |
| $(Na_{0.5}K_{0.5})NbO_3$ | 120 | −40 | 400 | 0.4 | 350 |

coefficient $\alpha_{ij}$ which is an axial second rank tensor. The transformation of the ME coefficient is given as following:

$$\alpha'_{il} = \pm|\alpha|\alpha_{ij}\alpha_{ij}\alpha_{jk}$$

In matrix form the transformation can be written as:

$$(\alpha') = \pm|\alpha|(\alpha)(\alpha)(\alpha)_t$$

The magnetoelectric tensor has nine independent coefficients. The effect vanishes for all symmetry groups containing time reversal symmetry (1′) and inversion $\left(\overline{1}\right)$ while space inversion along with time inversion $\left(\overline{1}'\right)$ is allowed. It can be shown that the effect is non-zero for 58 of the 90 magnetic point groups.

Sintered polycrystalline ceramics consisting of ferroelectric grains in the vicinity of ferromagnetic ones illustrates the importance of symmetry. For example, combining the magnetized $CoFe_2O_4$ ceramic having symmetry group $\infty/mm'$ with poled $BaTiO_3$ ceramic having symmetry group $\infty m'$ results in magnetoelectric $CoFe_2O_4$–$BaTiO_3$ ceramic having symmetry group $\infty m'$ [46]. Both $BaTiO_3$ and $CoFe_2O_4$ by themselves are not magnetoelectric. Thus, the ME effect can be realized by incorporating materials of suitable symmetry in a composite.

## 3 ME coupling coefficient

The upper limit for the value of the ME susceptibility can be given as:[49]

$$\alpha_{ij}^2 < \left(\kappa_{ii}^e \chi_{jj}^m\right) \tag{1}$$

where $\kappa^e$ and $\chi^m$ are the electric and magnetic susceptibilities respectively. A similar relationship can be derived based on the thermodynamic considerations given as:[50]

$$\alpha_{ij} < \left(\varepsilon_{ii}\mu_{jj}\right)^{1/2} \tag{2}$$

where $\varepsilon$ and μ are the electric permittivity and magnetic permeability respectively. The magnetoelectric coupling coefficient has been defined as:

$$k_{ME} = \frac{U_{mutual}}{\left(U_{electric}.U_{magnetic}\right)^{1/2}} \tag{3}$$

where $U_{mutual}$ (=$1/2\alpha_{ij}E_iH_j$, *where $H_j$ is the magnetic field*) is the mutual energy, $U_{electric}$ =$(1/2)\varepsilon_{ii}E_iE_i$ is the electric energy and $U_{magnetic}$ =$(1/2)\mu_{jj}H_jH_j$ is the magnetic energy. In order to evaluate the efficiency of energy conversion from magnetic to electric forms, or vice-versa, a working definition of the coupling coefficient can be written as:

$$k_{me}^2 = k_{ij,piezo}^2 k_{ij,magnetic}^2 \tag{4}$$

where $k_{ij,\ piezo}$ is the coupling coefficient of the piezoelectric phase, and $k_{ij,\ magnetic}$ is the coupling coefficient of the magnetic phase.

## 4 Magnetoelectric effect in composites synthesized via unidirectional solidification, sintering, and modified controlled precipitation route

### 4.1 Unidirectional solidification

The original work on in situ formation of ME composites was done at Philips Laboratories.The ME composites were prepared by unidirectional solidification of a eutectic composition of the quinary system Fe-Co-Ti-Ba-O [24, 25]. The eutectic composition was determined to be at 38 mol% $CoFe_2O_4$. Unidirectional solidification helps in the decomposition of the eutectic liquid into alternate layers of the constituent phases; a piezoelectric perovskite phase (P) and a piezomagnetic spinel phase (S) (L → P+S). Their results showed that excess of $TiO_2$ (1.5 wt %) gives a high ME voltage coefficient $dE/dH$=50 mV/cm·Oe. However, other compositions showed a lower $dE/dH$ in the range of 1–4 mV/cm·Oe. In a subsequent work, a high ME coefficient of 130 mV/cm·Oe was obtained in a eutectic

composition of $BaTiO_3$–$CoFe_2O_4$ by unidirectional solidification. This value is about an order of magnitude higher than that of the single crystal $Cr_2O_3$ ($dE/dH$=20 mV/cm·Oe).Unidirectional solidification requires critical control over the composition, especially when one of the components is a gas (oxygen). Recently Echigoya et al. synthesized a eutectic microstructure in this system through unidirectional solidification in a $N_2$ atmosphere [51]. Based on high resolution electron microscopy (HREM) studies, they arrived at the orientation relationships for this system as follows:

(a) For hcp $BaTiO_3$: (111) $CoFe_2O_4$//(001) $BaTiO_3$ and (110) $CoFe_2O_4$//(110) $BaTiO_3$; and
(b) For tetra/cubic $BaTiO_3$: (001) $CoFe_2O_4$//(001) $BaTiO_3$ and (100) $CoFe_2O_4$//(100) $BaTiO_3$.

Phase relations for the quinary system Ba-Ti-Ni-Fe-O have been studied using the $NiFe_2O_4$ and $BaTiO_3$ end components. Kramer et al. reported that $NiFe_2O_4$–$BaTiO_3$ (NF–BT) alloy system has characteristics of a pseudo-binary system and shows minima in the liquidus curve around 1,350–1,360 °C at the composition corresponding to 47–48 mol% NF [52]. The X-ray analysis of solidified samples below the liquidus minimum composition revealed the presence of only ferrite ($a$=8.339 Å) and perovskite ($a$=3.994 Å and $c$=4.038 Å) phases. Later, Boomgaard et al. also reported the presence of eutectic in this system [25]. The samples sintered in the range of 1,000–1,350 °C for fairly long periods of time (24 h) showed the presence of only ferrite and perovskite phases. A high ME voltage coefficient of 81.7 mV/cm·Oe was reported in their study for the composition given as 0.4 $BaTiO_3$–0.6 $Ni_{0.97}Co_{0.03}Mn_{0.10}Fe_{1.90}O_4$ sintered in oxygen atmosphere at 1,300 °C for 24 h.

Directional solidification, such as a Bridgman technique or floating zone method using single ellipsoid furnace, are complex involving tight control over the composition, cooling rate and temperature. On the other hand, sintered composites are easier and cheaper to fabricate with several advantages such as freedoms in the selection of constituent phases, their starting particle sizes, the sintering temperatures. Furthermore, sintering does not require the presence of eutectic or eutectoid transformations, and also provides the opportunity to combine phases with widely different crystal structures.

### 4.2 Sintering

In the past two decades, various particulate composites consisting of piezoelectric and magnetostrictive materials with different connectivity schemes including "3-0" and "2-0" have been reported: such as $CoFe_2O_4$–$BaTiO_3$, $NiFe_2O_4$–$BaTiO_3$, $LiFe_5O_8$–$BaTiO_3$, $CoFe_2O_4$–$Bi_4Ti_3O_{12}$, $CuFe_2O_4$–$PbZr_{0.53}Ti_{0.47}O_3$, etc [26–32]. Table 2 provides a brief list of results obtained on these composite materials. The primary requirement for synthesis of composites using the sintering route can be summarized as: (1) individual phases should be in equilibrium, (2) mismatch between grains should not be present, (3) large magnetostriction and piezoelectric effects in the respective constituent phases, (4) high dielectric insulation so that accumulated charge does not leak through the composite, and (5) the ability to pole the piezoelectric phase in the composite.

Ryu et al. have investigated the effect of the sintering temperature on the sintering behaviors, microstructures, piezoelectric, and ME properties of particulate composites constituting Ni-ferrite doped with Co, Cu, Mn particles in a PZT matrix [53, 54]. It was found that not only the connectivity of the ferrite phase but also the sintering temperature are the important parameters for realizing higher ME voltage coefficient. Figure 3 shows the maximum ME voltage coefficient of various composition as a function of sintering temperature [54]. A high ME voltage coefficient of 115 mV/cm·Oe at 1 kHz was reported from the composites of 20% ferrite modified PZT sintered at 1,250 °C: these excellent results were attributed to a homogeneous and well-dispersed microstructure, high resistivity, and large grain size of the matrix PZT phase [54]. At low frequencies and DC bias fields the magnitude of the ME coefficient from the bulk sintered composites was on the order of 50–100 mV/cm·Oe. Hot-pressed samples exhibited an order of magnitude improvement in the ME voltage coefficient, as compared to the sintered samples [27].

An important parameter in the selection of the composite constituent phases is interface coupling ($k$) between the piezoelectric and magnetostrictive phases, which can vary significantly with the dopant concentration [55–57]. It has been reported that $NiFe_2O_4$ provides an ideal interface coupling with PZT ($k$=1); while $La_{0.7}Sr_{0.3}MnO_3$, $La_{0.7}Ca_{0.3}MnO_3$, and $CoFe_2O_4$ exhibit poor coupling ($k \leq 0.1$) with it. Substitution of Zn in the ferrites has a positive effect on the coupling which has been attributed to the release of the intrinsic lattice strain incurred during the sintering. The ME voltage coefficient was found to increase by a factor of 5 by replacing 40% Co with Zn, and by a factor of 1.5 by replacing 20% Ni with Zn. It has also been suggested that a soft magnetic material with high permeability and low magnetic anisotropy might provide an enhanced value of k by assisting the movement of domain walls. Experimental results on the Zn-modified ferrites have confirmed this suggestion [56].

Recently, the system PZT–Ni/Co/Li Ferrite was revisited by Bichurin et al. who studied the effect of electromechanical resonance on the magnitude of ME coefficient. They found a giant enhancement in the magnitude of the bulk composites at the resonance frequency of the samples. A high ME coefficient of 23,000 mV/cm·Oe was reported for the samples with 80% PZT–20% Ni Ferrite (~350 kHz,

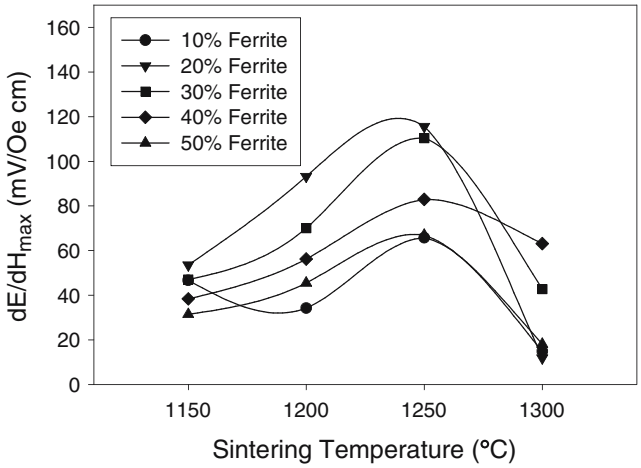


**Fig. 3** Maximum ME voltage coefficient of the PZT and Ni-ferrite particulate composites as functions of sintering temperature and Ni-ferrite particle contents

sample diameter 10 mm), an increase by a factor of 600 as compared to the data at low frequency (~1 kHz) [34]. In this study it was also found that the increase in the magnitude of ME coefficient at resonance is much higher in the sintered samples as compared to the laminated composites.

In spite of several advantages, the sintered composites provide an inferior response as compared to hot pressing or unidirectional solidification. For example, an in situ grown eutectic composite in the system $BaTiO_3$–$CoFe_2O_4$ exhibited ME coefficient of 130 mV/cm·Oe while the same composition in the sintered form exhibited ME coefficient of <10 mV/cm·Oe [25]. The hot pressed samples of PZT/$Ni_{0.8}Zn_{0.2}Fe_2O_4$ provided one order magnitude higher ME response as compared to sintered samples. Thus, a more appropriate synthesis route will be the one which can combine the advantages of both the unidirectional solidification and sintering methods.

### 4.3 Modified controlled precipitation route

Higher ME coefficients imply higher elastic coupling between the magnetic and piezoelectric phases. The elastic coupling can be maximized by having coherent response from the magnetostrictive phase under dc bias, so that the stress on the piezoelectric lattice across the grains is in phase with each other. This is only possible if there is uniform distribution of the magnetostrictive phase in the piezoelectric matrix. If the particles are crystallographically aligned with the matrix lattice, more benefits can be obtained because of the built-in directionality. The precipitation method, commonly utilized in metallic alloys, has the potential for producing such a structure with extremely simple and cost-effective processing. Our study has focused on the application of the precipitation technique to the sintered magnetoelectric ceramics with the objective of achieving a strong coupling between ferroelectric and magnetic order parameters.

Figure 4 illustrates the principle of the controlled precipitation route and the synthesis process. Figure 4a shows a hypothetical phase diagram forming eutectic between the

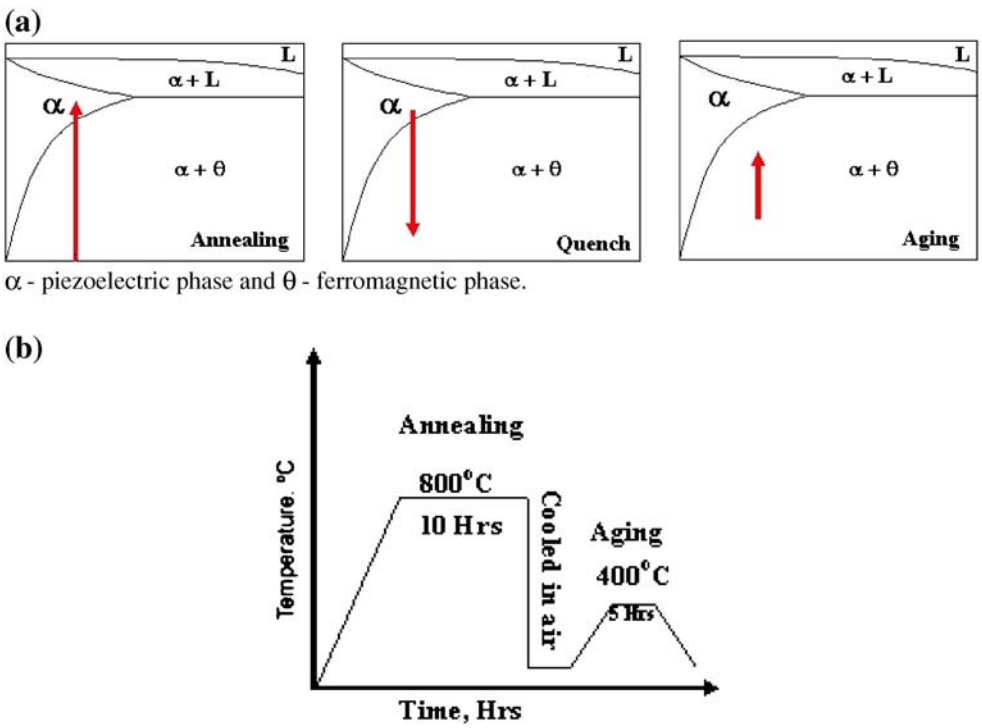


**Fig. 4** **a** Hypothetical phase diagram illustrating the principle of controlled precipitation route, and **b** the temperature profile of the post sintering thermal treatment. Annealing and aging treatments can be varied for optimization

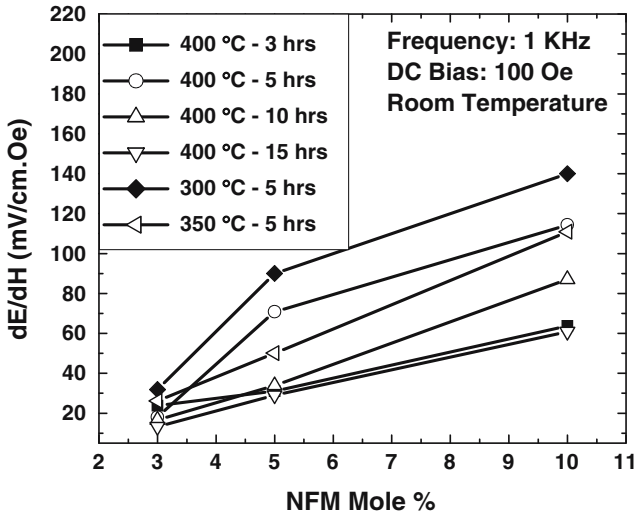


**Fig. 5** Magnetoelectric coefficient for the PZT–NFM system illustrating the effect of the aging temperature. All the samples were annealed at 800 °C for 10 h

end components. A composition corresponding to the arrow shown on this diagram when subjected to the thermal treatments of annealing (in the single phase region, $\alpha$), quenching in two phase region ($\alpha+\theta$), followed by aging in two phase region has the possibility of producing $\theta$ precipitates in the $\alpha$ matrix. The quenched ($\alpha'$) phase is a metastable supersaturated solution having the same crystal structure as $\alpha$ but with the composition farther from the equilibrium. On aging, the solution goes through the transformation, $\alpha' \rightarrow \alpha+\theta$.

Based on this principle we designed the synthesis route for the $Pb(Zr_{0.52}Ti_{0.48})O_3$ (PZT)–$NiFe_{1.9}Mn_{0.1}O_4$ (NFM) system [58]. Figure 4b shows the post sintering thermal treatment used for fabricating PZT–NFM. The unidirectional quenching was achieved by enclosing the samples in an alumina tube and rapidly moving the tube out of the hot zone in the furnace. Figure 5 shows the magnetoelectric data for various NFM content at different aging temperatures and time. This data clearly demonstrates the success of this synthesis technique in modulating the magnetoelectric properties. Using this method, an ME coefficient of 120 mV/cm·Oe was obtained from the PZT–10 NFM sample aged at 300 °C for 3 h [59].

Figure 6a shows the microstructure of the samples sintered at 1,125 °C for compositions PZT–5NFM at 20 kX magnification [59]. A dense microstructure for all compositions was obtained. Elemental analysis using the EDX showed that NFM grains are randomly distributed in the piezoelectric matrix. Figure 6b shows the microstructure of the PZT–5NFM after annealing and aging at 400 °C for 5 h [58]. An immediate observation of the images of sintered and aged sample provides noticeable difference in the distribution of the NFM particles. An even distribution of NFM particles was observed after the aging treatment. Elemental X-ray mapping showed that nickel and iron are distributed in the whole matrix but in certain areas (black regions) their concentration is higher than the surrounding [60]. Figure 7a and b shows the TEM investigations on PZT–5NFM annealed and aged samples respectively. The microstructure showed the redistribution of the spinel phase after aging as indicated by the arrow on the figure. Figure 8a and b compares the PFM images of the sintered and aged PZT–5NFM samples. Comparing the two PFM images it can be seen that annealing and aging treatment results in the homogenization of the magnetic domain distribution. Assuming that spinel phase is single domain it can be hypothesized that the annealing and aging treatment results in redistribution of the magnetic phase.

Results reported on the ME composites synthesized using this technique have indicated an enhancement by 50% in the magnitude of the ME coefficient. It has been

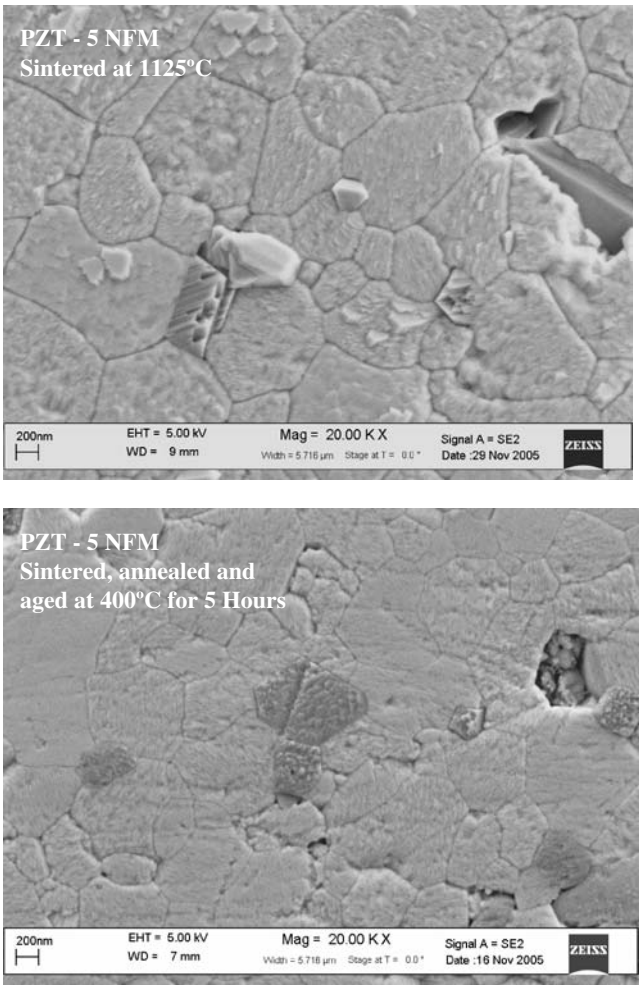


**Fig. 6** SEM microstructure of PZT–5NFM at different conditions **a** sintered sample at 20 kX magnification, and **b** sintered, annealed and aged sample at 20 kX magnification

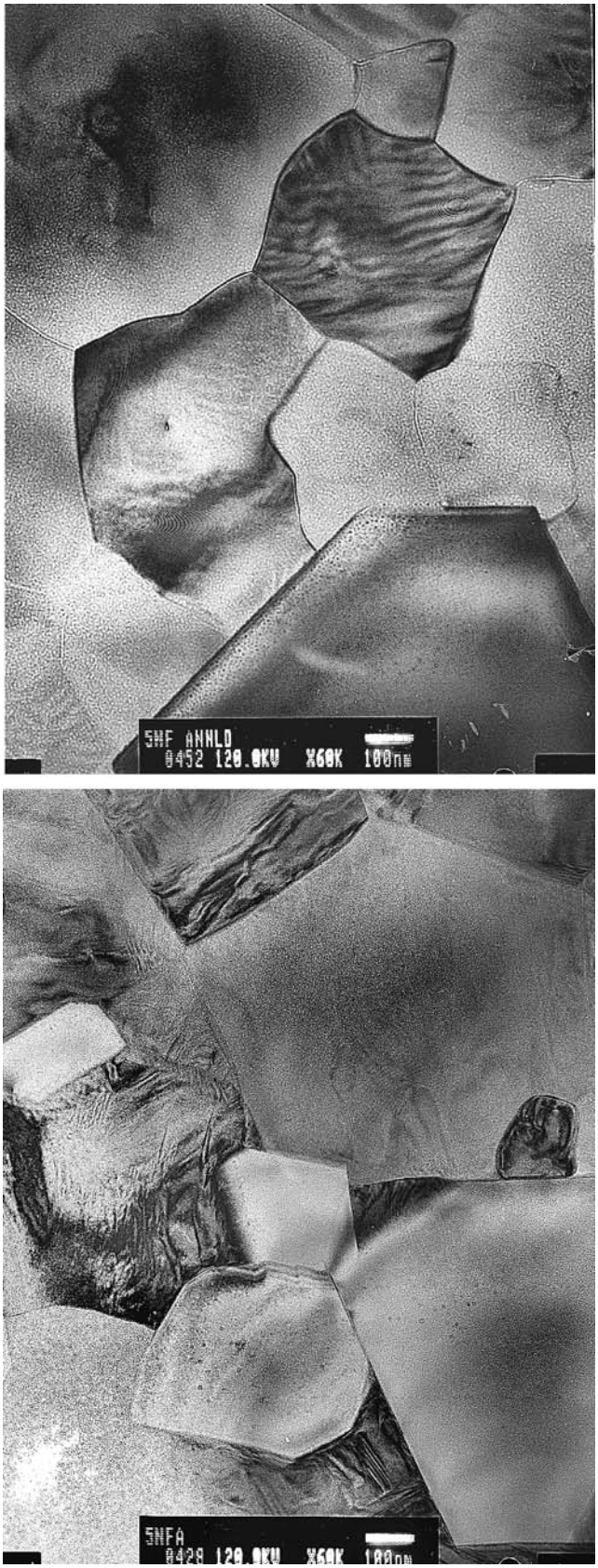


**Fig. 7** TEM microstructure of PZT–5NFM at various conditions. **a** Annealed at 800 °C for 10 h and **b** aged at 400 °C for 5 h

mentioned that controlled precipitation route has following advantages over the sintering techniques including: [58–60]

(1) Ability to synthesize bulk material with crystallographically aligned nanoscale interfaces—ordered distribution of one phase in another.
(2) Ability to synthesize material with high interfacial area—higher interphase elastic coupling.
(3) Ability to thermally control the microstructure and as a result properties of the material—large range of values for dielectric permittivity and magnetic permeability can be obtained from same composition.
(4) Ability to synthesize grain oriented material—large anisotropic properties.

## 5 Magnetoelectric effect in laminate composites

Compared with particulate composites, the laminated magnetostrictive and piezoelectric composites have shown much stronger magnetoelectric coupling. Laminate composites are generally fabricated by bonding magnetostrictive and piezoelectric layers using the silver epoxy, followed by annealing at a lower temperature of ~100 °C. The most common geometry in laminate composites is a "sandwich" structure, whereby the piezoelectric layer is arranged between two magnetostrictive ones. Magnetoelectric behavior in laminate composites has been reported for various material couples including $Pb(Zr,Ti)O_3$ (PZT) or $Pb(Mg_{1/3}Nb_{2/3}O_3$–$PbTiO_3$ (PMN–PT) layers laminated with magnetostrictive $Tb_{1-x}Dy_xFe_{2-y}$, Permendur, $Ni_{1-x}Co_xFe_2O_4$ (i.e., NFO), or $Co_{1-x}Zn_xFe_2O_4$ (i.e., CFO) ones [56, 57, 61–72]. Recently, we also developed new ME laminate composites of magnetostrictive Fe-20at%Ga crystals with piezoelectric PZT ceramics and piezoelectric single crystals that exhibited a large magnetoelectric (ME) coupling [73, 74]. Fe-Ga/PZT or Fe-Ga/PMN-PT laminates also exhibited strong ME effects under dc magnetic bias. Figure 9a and b shows the induced ME voltages in Fe-Ga/PMN-PT laminates as a function of magnetic field bias $H_{dc}$ for (1) longitudinal magnetization and longitudinal polarization and (2) longitudinal magnetization and transverse polarization modes. The maximum ME voltages for Fe-Ga/PMN-PT laminates for the two modes are 1.41 V/Oe (1.01 V/cm−Oe) and 30 mV/Oe (0.6 V/cm−Oe), respectively.

It is well known that both piezoelectric and magnetostrictive resonators have high coupling (electromechanical and magnetomechanical, respectively) resonance effects. Accordingly, ME resonators driven near their resonance frequency should also have a significantly higher ME coupling, relative to laminates driven off-resonance. Our measured results show that ME voltage coefficient for a Fe-Ga/PMN-PT laminate is dramatically

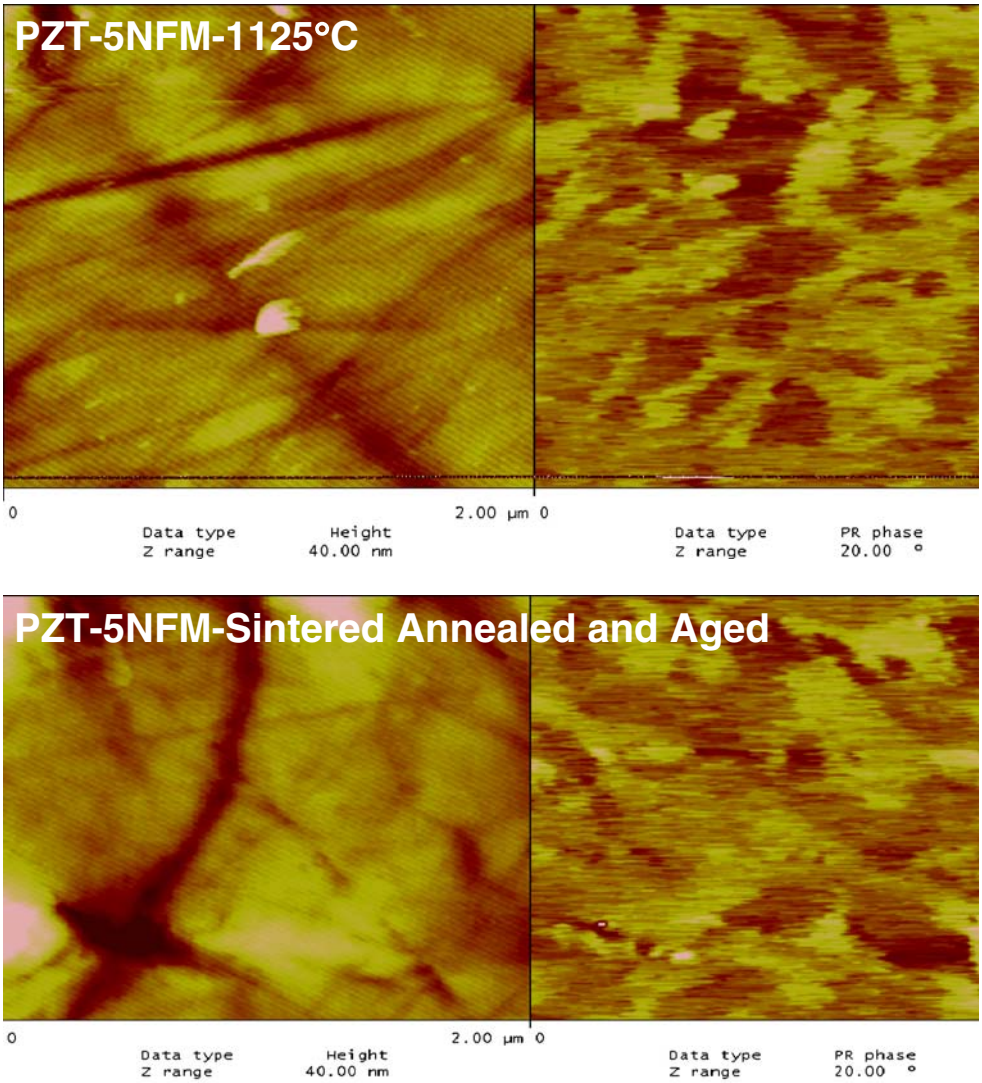


**Fig. 8** PFM images of PZT-5NFM at various conditions. **a** Sintered at 1,125 °C for 3 h and **b** annealed at 800 °C for 10 h followed by aging at 400 °C for 5 h

increased when operated at resonance frequency. The maximum value of the ME coefficient for longitudinal magnetization and longitudinal polarization mode is 50.7 V/Oe (or 36.2 V/cm−Oe), which is almost 40 times higher than that in low-frequency range. Whereas the ME maximum value for longitudinal magnetization and transverse polarization mode is 3.6 V/Oe (or ~70 V/cm−Oe). Figure 10 illustrates this strong resonance ME response.

Recently, results have also been reported for the metal—PZT laminate composites. The study of Narendra et al. indicated that the arrangement Ni/PZT/Ni provided higher ME coefficient of 8.5 mV/cm·Oe compared to Fe/PZT/Fe which exhibited magnitude of 4.5 mV/cm·Oe at 1 kHz and 1,000 Oe DC bias [75]. The results on the Fe-PZT-Fe showed that this composite exhibited unique features of zero crossing and sign reversal. Investigations by Laletin et al. have shown that the low frequency (1 kHz) transverse magnetoelectric coefficient in the laminate composites of Ni/PZT/Ni is of the order of ~400 mV/cm·Oe [76]. Further it was reported that at the resonance frequency of 260 kHz the same composite exhibited the transverse ME coefficient of 90 V/cm·Oe.

## 6 Magnetoelectric effect in piezoelectric polymer/magnetostrictive composites

Nan et al. have fabricated the three phase composite consisting of PZT and Terfenol-D powders in the PVDF matrix using a hot moulding technique [77–79]. Initially, PZT and Terfenol-D powders were mixed with PVDF and the mixture was then hot-pressed into a three-layer stack of PZT/Terfenol-D/PZT at 190 °C. In these three phase composites, PVDF is used as a binder which is inert and suppresses losses by eddy currents, while PZT and Terfenol-D are embedded in the polymer matrix. The strain resulting from the magnetostriction of Terfenol-D particles

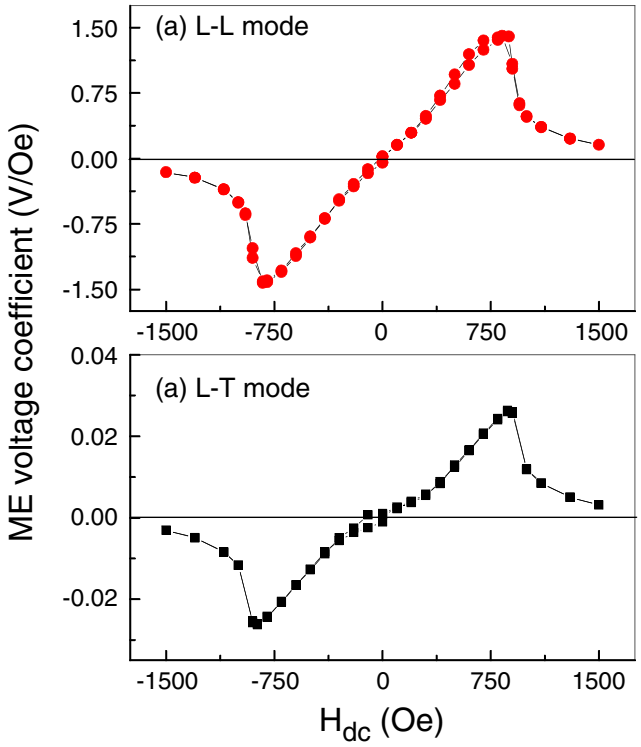


**Fig. 9** ME voltage coefficients as a function of $H_{dc}$ for the L-L mode and L-T mode of Fe-Ga/PMN-PT laminates. The driving ac magnetic field was $H_{ac}$=1 Oe (amplitude) and the measurement frequency $f$=$10^3$ Hz

passes through the polymer matrix along to PZT particles, resulting in induced polarization changes. The experimental results showed that a percolation transition occurs for Terfenol-D volume fraction of $f$~0.12 in the composite. For $f$<0.07, the dielectric and piezoelectric properties vary only slightly with $f$; and that $\varepsilon_{33}$=200, tan$\delta$=0.02, and $d_{33}$=62 pC/N. The maximum magnitude of the ME coefficient was found to be 42 mV/cm·Oe for $f$=0.06 at a DC bias of 2,000 Oe [77]. The magnitude of the ME coefficient was limited mainly by the value of the percolation threshold of the Tefenol-D phase.

## 7 Operational principles of ME laminate, and modeling of responses

### 7.1 Magnetoelectric (ME) working modes

In magnetostrictive/piezoelectric laminate composites, the layers of the bi-material are stress-coupled. When the magnetostrictive layers are strained under an ac magnetic field ($H_{ac}$), the piezoelectric layers under go forced oscillation. Consequently, an electric field E (or voltage) is induced across the piezoelectric layer due to piezoelectricity. This elastically coupled response between an applied H and an induced E (or vice versa) is known as the magneto-(elasto)-electric (or ME) effect. The various modes for rectangular types of ME laminates are illustrated in Fig. 10. When both the applied H and the induced E are parallel to the principle vibration mode, the ME laminate can be said to operate in its (L-L) mode (see Fig. 11a). When the applied H is perpendicular to the principle mode and the induced E parallel to it, the ME laminate operates in its (T-L) mode (see Fig. 11b); whereas, when H is applied parallel to the principle direction and the induced E measured perpendicular to it, the laminate operates in its (L-T) mode (see Fig. 11c). And, finally, when both the applied H and induced E are perpendicular to the principle mode, the laminate operates in its (T-T) mode (see Fig. 11d).

### 7.2 Equivalent circuit for ME coupling [80, 81]

Magnetoelectricity occurs in laminates as a bi-effect between layers, due to stress–strain coupling of the layers. For a rectangular ME laminate, when an ac magnetic field $H_{ac}$ is applied along the length or thickness direction in the laminate, a longitudinal piezomagnetic vibration mode will be excited. Because the layers of the bi-material are stress coupled, a voltage is then induced on the piezoelectric plate. Accordingly, two sets of linear constitutive equations (small signal excitations) are required to describe the laminate as following:

$$\left.\begin{aligned} S_h^{(m)} &= s_{hk}^H T_k^{(m)} + d_{jh,m} H_j^{(m)} \\ B_i^{(m)} &= d_{ik,m} T_k^{(m)} + \mu_{ij}^T H_j^{(m)} \end{aligned}\right\} \begin{pmatrix} \text{piezomagnetic equation} \\ \text{in magnetic phase} \end{pmatrix} \tag{5}$$

$$\left.\begin{aligned} S_h^{(p)} &= s_{hk}^D T_k^{(p)} + g_{gh} D_j^{(p)} \\ E_i^{(p)} &= -g_{ik} T_k^{(p)} + \beta_{ij}^T D_j^{(p)} \end{aligned}\right\} \begin{pmatrix} \text{piezoelectric equation} \\ \text{in piezoelectric phase} \end{pmatrix} \tag{6}$$

$(h,\ k = 1, 2, \ldots, 6;\ i,j = 1, 2, 3)$

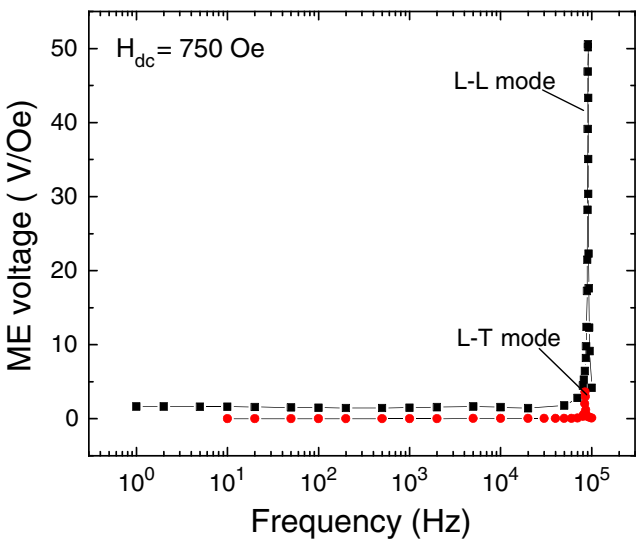


**Fig. 10** Resonance ME response of ME Fe-Ga/PMN-PT laminate at $H_{dc}$=750 Oe

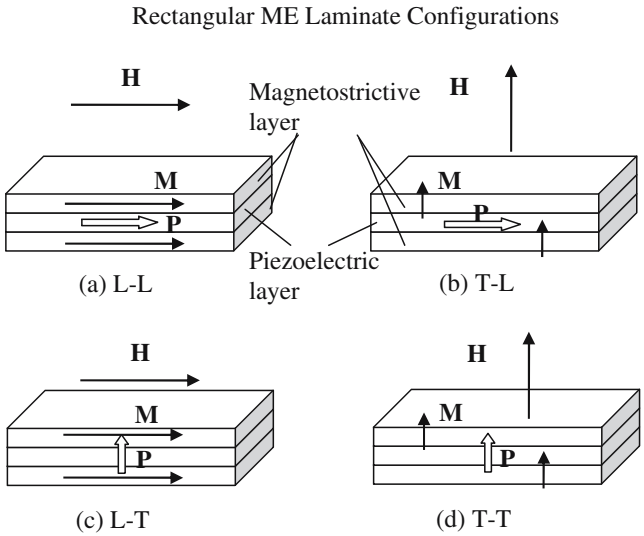


**Fig. 11** Various modes of rectangular-type ME laminates

In Eq. 5, $H_j^{(m)}$ and $B_i^{(m)}$ are magnetizing and magnetic induction component fields, respectively. $S_k^{(m)}$ and $T_k^{(m)}$ are strain and stress components in magnetostrictive material layers; $S_{hk}^H$, $d_{jh,m}$ and $\mu_{ij}^T$ are elastic compliance constant component at constant magnetic field $H$, piezomagnetic constant, and magnetic permeability at constant stress in the magnetostrictive material, respectively. In Eq. 6 $D_j^{(p)}$ and $E_i^{(p)}$ are electric displacement and electric field components in piezoelectric material layer; $S_h^{(p)}$ and $T_k^{(p)}$ are strain and stress components in piezoelectric layer; $s_{hk}^{(D)}$, $g_{jh,p}$ (or $g_{ik,p}$) and $\beta_{ij}^T$ are elastic compliance constant at constant electric displacement, piezoelectric voltage constant, and dielectric impermeability, respectively. These two sets are mutually coupled through an equation of motion, because they vibrate together:

$$\left(\Delta m^{(p)} + \Delta m^{(m)}\right)\frac{\partial^2 u}{\partial t^2} = \Delta T^{(p)} A^{(p)} + \Delta T^{(m)} A^{(m)} \qquad (7)$$

where $\Delta m^{(p)}$ and $\Delta m^{(m)}$ are mass units in piezoelectric layer and magnetostrictive layers, respectively; $u$ indicates displacement excited by external magnetic field $H^{(m)}$; and $A^{(p)}$ and $A^{(m)}$ are cross sectional areas of piezoelectric layer and magnetostrictive layers in the laminate, respectively. Consequently, a magneto-elasto-electric equivalent circuit can be obtained, which can be employed to predict the ME coefficients.

Figure 12a and b illustrate the magneto-elasto-electric equivalent circuits for one-dimension L-L and L-T modes, respectively. In these circuits, an applied H produces a mechanical force or "mechanical voltage" via the magneto-elastic coupling factor $\varphi_m$, and subsequently an electrical voltage V across the piezoelectric layer due to electromechanical coupling. In the circuits, a transformer with a turn-ratio of $\varphi_p$ is used to represent the electromechanical coupling. Solving this equivalent circuit, the low-frequency ME voltage coefficients for L-L and L-T modes are found to be given as:

$$\left|\frac{dV}{dH}\right| = \left|\frac{\varphi_m \varphi_p}{j\omega C_0 Z}\right| \qquad (L - L \mod e) \qquad (8)$$

$$\left|\frac{dV}{dH}\right| = \left|\frac{\varphi_m \varphi_p}{j\omega C_0\left(Z + \varphi_p^2 / j\omega C_0\right)}\right| \qquad (L - T \mod e) \qquad (9)$$

The calculated values based on Eqs. 8 and 9 were much higher than measured values, because electric and magnetic losses, and sliding loss in bonding interfaces were not considered in Eqs. 5, 6, and 7. In our prior reports [64, 72] we modified above equations by introducing a factor, β, and the predictions were close to measured ones in some extents.

In addition, from the derived ME equivalent circuits, the effective ME coupling coefficient, $k_{\text{mag-elec}}$(eff), as a function of the geometric parameter $n_m$ (magnetostrictive layer) for a laminate of piezoelectric PZT-8 and magnetostrictive Terfenol-D, could be calculated, as shown in Fig. 13. When $n_m$=0, this laminate composite contains no magnetostrictive material, thus $k_{\text{mag-elec}}$(eff) is zero. Correspondingly, when $n_m$=1, the laminate contains only

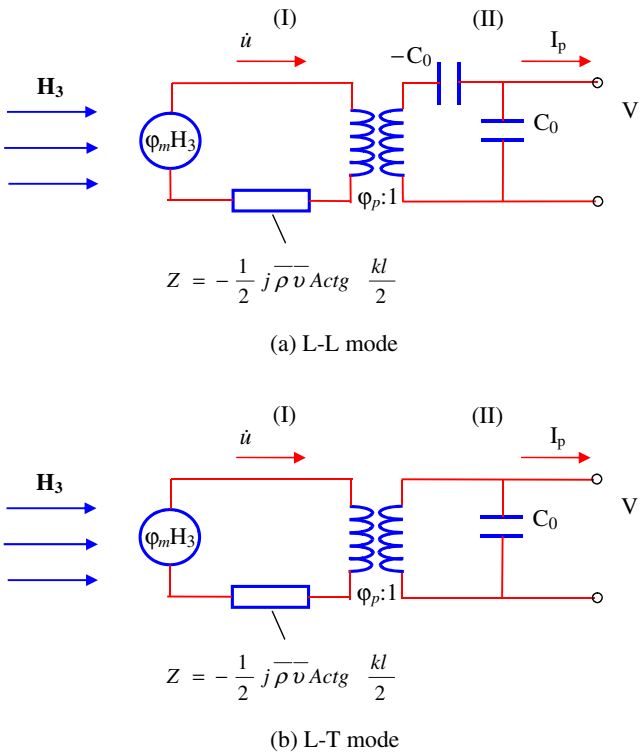


**Fig. 12** Magneto-elastic-electric bi-effect equivalent circuits for **a** L-L mode and **b** L-T mode

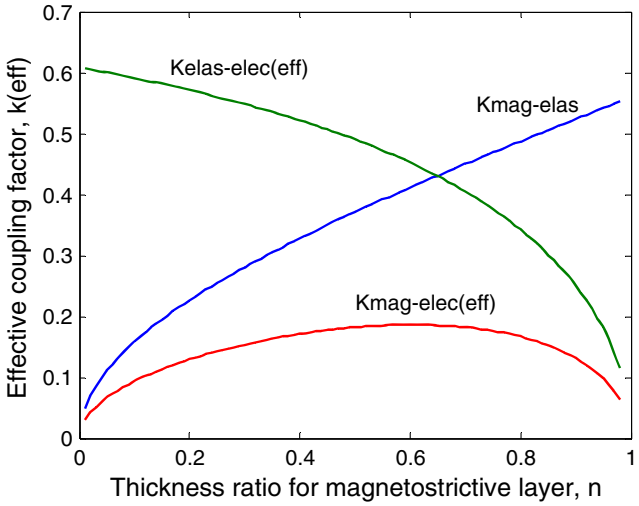


**Fig. 13** Calculations for effective magneto-elastic, elasto-electric and magneto-electric coupling factor

magnetostrictive material, and again $k_{\text{mag-elec}}(\text{eff})$ is zero. Between these two geometric limits, a maximum value of $k_{mag\text{-}elec}(eff)$ can be found. The optimum geometric parameter, $n_{\text{m,opt}}$ for a L-L mode [82] is

$$n_{\text{m,opt}} = \frac{1}{1+\gamma\left(1+8k_{33\text{m}}^2/\pi^2\right)^{1/2}} \tag{10}$$

where $\gamma = \frac{S_{33}^D}{S_{33}^B}$ is a ratio of the compliance constants of the piezoelectric and magnetostrictive layers.

In a L-T mode, there is also an optimum geometric parameter, $n_{\text{m,opt}}$ for the terfenol-D layers, which results in a maximum ME voltage coefficient $\text{d}V/\text{d}H_{\text{L-T}}$:

$$n_{\text{optim}} = \frac{1}{1+\sqrt{\alpha}} \tag{11}$$

where $\alpha = \left(1-k_{31,\text{p}}^2\right)\frac{S_{11}^E}{S_{33}^H}$ is also a ratio of the compliance constants of the piezoelectric and magnetostrictive layers.

At electromechanical resonance ($\omega=\omega_s$), $\text{d}V/\text{d}H$ (for example: a L-L mode) reaches a maximum value of

$$\left(\frac{\text{d}V}{\text{d}H}\right)_{\omega s} = \frac{4Q_{\text{m}}\varphi_{\text{m}}\varphi_{\text{m}}}{\pi Z_0\omega_{\text{s}}C_0} \tag{12}$$

where $Q_{\text{m}}$ is the effective mechanical quality factor of the laminate composite including contributions from the Terfenol-D and piezoelectric layers, and the bonding between the layers. Analysis has shown that $\text{d}V/\text{d}H$ at the resonance frequency is $\sim Q_{\text{m}}$ higher than that at sub-resonant frequencies.

## 8 Applications

In the past few years, several applications have emerged for magnetoelectric materials including power harvesting, current transformers, phase shifters, magnetic field sensors, current sensors, filters, and resonators. We mention some of these applications below.

### 8.1 Power harvesting

Magnetoelectrics can be used to generate power from a stray magnetic field in an industrial environment as schematically depicted in Fig. 14a. An oscillating magnetic field present in the surrounding will induce an AC stress on the piezoelectric layer through magnetostriction. The stress will be converted into electric charge at the piezoelectric layer through a direct piezoelectric effect which can be processed by the circuit. Magnetoelectrics can also be used to convert the vibration energy into electricity. In a simple design, vibrations can be used to rotate a mechanical assembly which consists of magnets, thereby creating an oscillating magnetic field. Ferro Solutions has recently demonstrated a device based on this approach as shown in Fig. 14b [83]. This device is able to provide an energy density of 2.0 mW per cubic inch with vibrations of 21 Hz and 100 mg. These devices could find use in applications such as structural health monitoring and condition based maintenance. A windmill based on the above approach is under development at The University of Texas Arlington.

### 8.2 High sensitivity magnetic sensors

A highly sensitive magnetic field sensor can be designed using the laminate geometry. In this construction, when a magnetic field is applied to the magnetostrictive layer, it strains; thus producing a proportional charge in the piezoelectric layer. In another version, a magnetic field sensor can be developed by bonding a field-annealed metallic glass ribbon onto a resonating piezoelectric plate with a viscous fluid. An AC voltage is applied to the piezoelectric plate which produces a longitudinal stress field. With proper bonding techniques, the dynamic stress in the metallic ribbon is congruent with that in the piezoelectric while the static component is eliminated through the viscous fluid. The dynamic stresses create an oscillating electromotive force (e.m.f.) in the surrounding pick-up coil through the Villari effect. When exposed to low-frequency magnetic fields, a low-frequency e.m.f. is generated in the coil which is extracted from the carrier e.m.f. with conventional phase sensitive detection techniques. The measured detection limits can reach up to $6.9\times10^{-6}$ A/m at 1 Hz which compares with that of fluxgate magnetometers [84].

In our research, both Terfenol-D/PMN-PT and Fe-Ga/PMN-PT laminates have shown high magnetic field sensitivity. Figure 15 shows the induced voltages across the two ends of a PMN-PT layer in the ME laminate as a

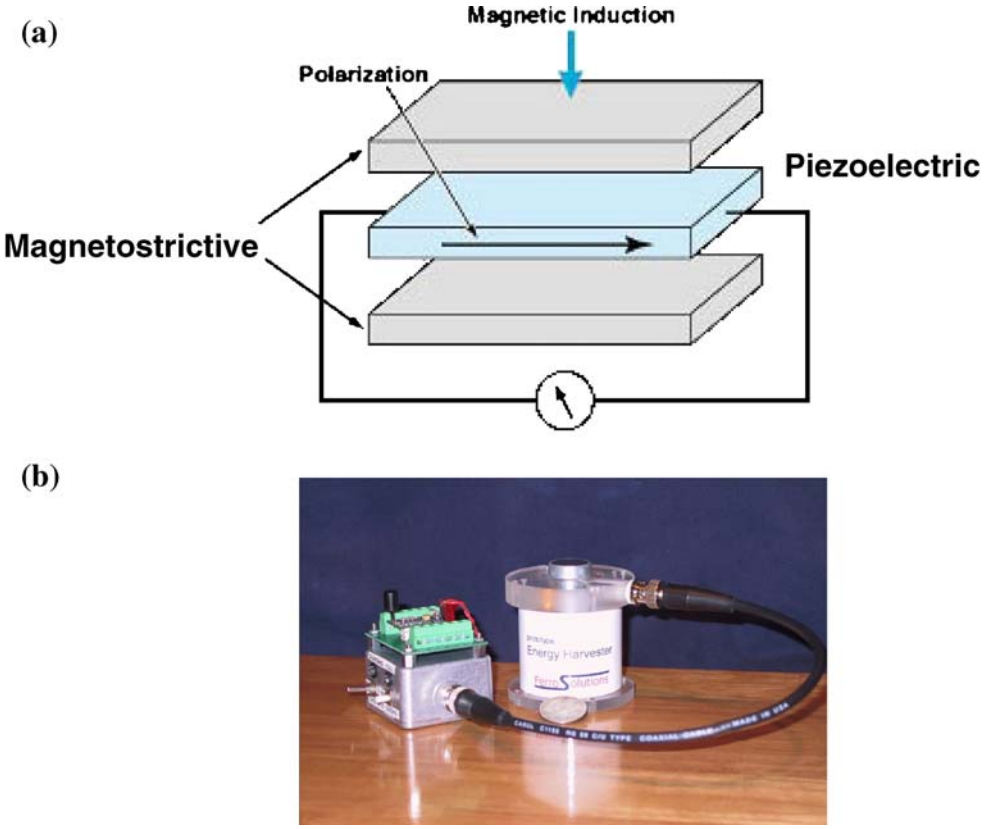


**Fig. 14** **a** Schematic of the electrical assembly for power harvesting from stray magnetic fields. **b** Magnetoelectric vibration energy harvesting device fabricated by the Ferro Solutions (Taken from the website: http://www.ferrosi.com/products.htm)

function of ac magnetic field ($H_{ac}$) at a drive frequency of 1 kHz under a given dc magnetic biase ($H_{dc}$). The data was measured using a lock-in amplifier method. For comparisons, the ME voltage coefficients for both L-L and L-T modes are illustrated. In this figure, the induced ME voltage can be seen to have a linear response as a function of $H_{ac}$ over a wide field range from ~$10^{-11}$ Tesla (or $10^{-7}$ Oe) to ~$10^{-3}$ Tesla (or 10 Oe) [66, 67, 74]. When the laminates were operated at resonance, the magnetic field that could be detected was about $10^{-12}$ Tesla. The measurements were performed at ambient conditions. These results unambiguously demonstrate that ME laminates have an ultra-high sensitivity to small magnetic field variations.

Ueno and Higuchi have reported a highly sensitive heat-resistant magnetic sensor using laminate composites as shown in Fig. 16 [85]. In this case the laminate composite consisted of a magnetostrictive layer (Terfeno-D) bonded with two piezoelectric layers (Lithium Niobate) plates. The magnetostrictive layer used as a ground electrode was grain oriented in $X$ direction, while the piezoelectric plates are alternately poled in the $Z$ direction. The magnetic sensor in the composite was integrated into a magnetic circuit with a permanent magnet and iron yokes. The sensor works on the principle that a detectable yoke displacement is transduced into a voltage on the piezoelectric material. The magnetic circuit assists in efficient conversion of the magnetic energies and converting a mechanical displacement into a voltage across the piezoelectric plates. The sensor was reported to have a sensitivity of 50 V/mm with an operating temperature range of over 200 °C [85]. This sensor could find applications in detecting ferromagnetic objects in high temperature environments, such as that in automobiles and industrial machinery.

Quandt et al. reported a magnetic field (vector) sensor using Fe-Co/Tb-Fe multilayers on piezoelectric PMN-PT single crystals. Four micron thick multilayer structures of

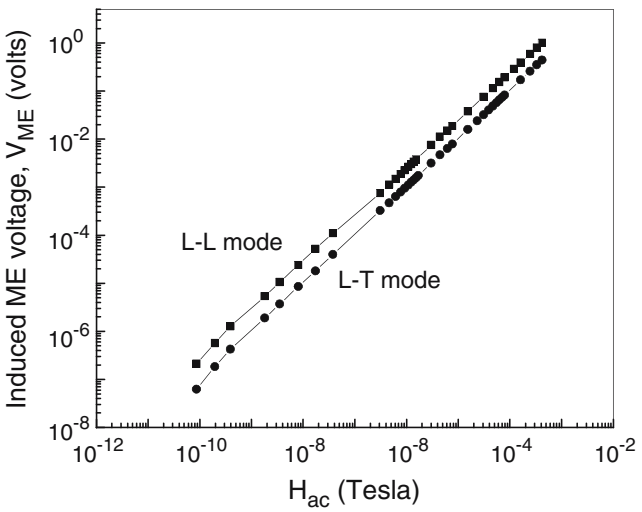


**Fig. 15** Limit magnetic field sensitivity of Terfenol-D/PMN-PT ME laminate

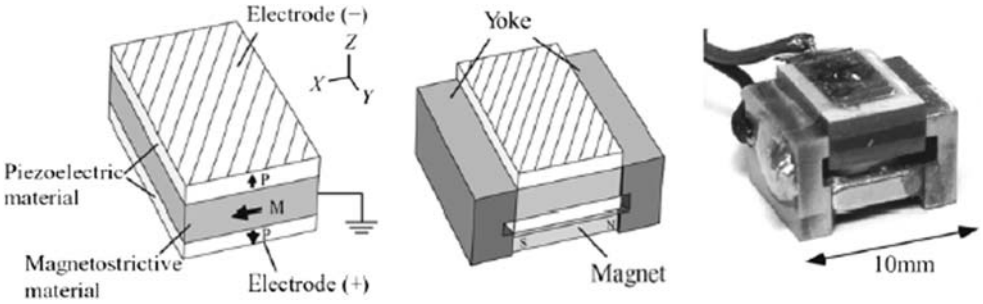


**Fig. 16** High temperature magnetic sensor using laminates of Terfenol-D and lithium niobate (© 2005 IEEE, taken from [85]

(Tb-Fe 7 nm/Fe-Co 10 nm)$_x$ were fabricated by sputtering [86]. The polarization axis of the piezoelectric substrate was aligned transversely to the crystal plane (*Z* axis). The magnetoelectric response of the structure was found to be ~7 mV/cm−Oe along the 'hard' *X* axis. It was reported that by annealing the films at 275 °C and subsequently cooling them in a magnetic field of 220 mT applied along the easy *Y* axis that in-plane anisotropy was created thereby increasing the ME effect to 10 mV/cm·Oe along the *X* axis. The sensitivity at the maximum ME voltage coefficient was found to differ by a factor of 4 between the hard and easy axes, whereas the sensitivity normal to the plane was not distinguishable from background noise.

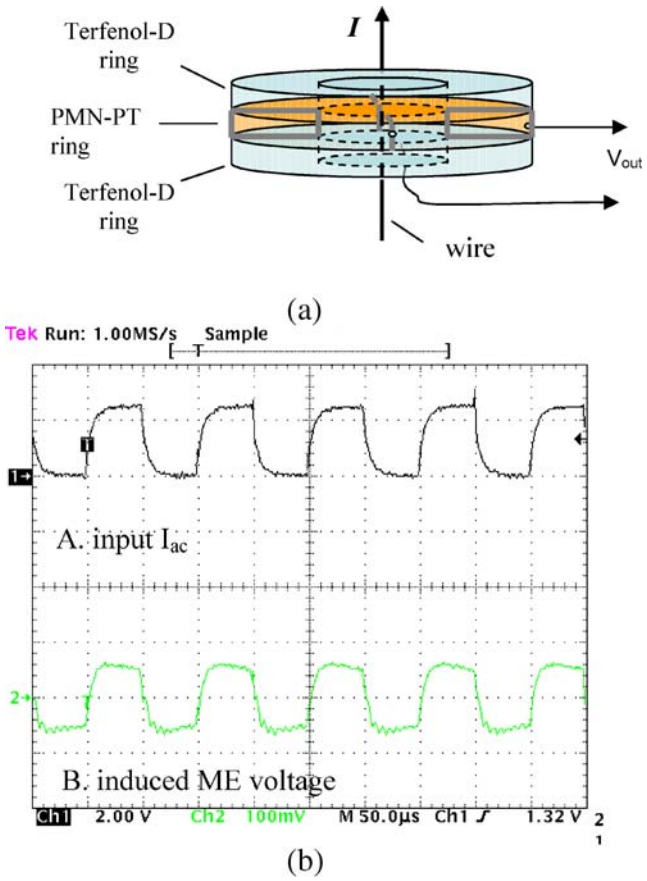


**Fig. 17** ME current sensor: **a** Ring-type ME laminate and **b** square-wave current detection

## 8.3 Current sensors

It is well known that a straight wire containing ac or dc current $\boldsymbol{I}$ will excite an ac or dc vortex magnetic field $\boldsymbol{H}_{vor}$ around this wire. Therefore, a ring-type magneto-electric laminate composite [65, 70] should be a suitable design for vortex magnetic detection, or current $\boldsymbol{I}$ detection because of $\boldsymbol{H}_{vor}=I/\pi r$ ($r$: radius of vortex magnetic field). We have designed a ME ring-type laminate made of circumferentially-magnetized magnetostrictive TERFENOL-D and a circumferentially-poled piezoelectric Pb(Zr,Ti)$O_3$ (PZT) or PMN-PT (similar a L-L mode), which have been shown to have a high sensitivity (up to 5.5 V/cm·Oe at low-frequency) to a vortex magnetic field. At room temperature, an induced output voltage from this ring laminate exhibited a near linear response to an ac vortex magnetic field $\boldsymbol{H}_{vor}$ over a wide magnetic field range of $10^{-12}<\boldsymbol{H}_{vor}<10^{-3}$ Tesla (or current: $10^{-7}<\boldsymbol{I}<10$ A) at frequencies between Hz and kHz. Figure 17a illustrates a ring-type ME laminate, and Fig. 17b shows the ME voltage response to a square-wave current passing the wire. The detection using a toroidal type variable reluctance coil ($N$=100 turns) exhibited much smaller induced voltage (by a factor of 0.01 times) than that of our ME ring sensor. Also, for the reluctance coil, the

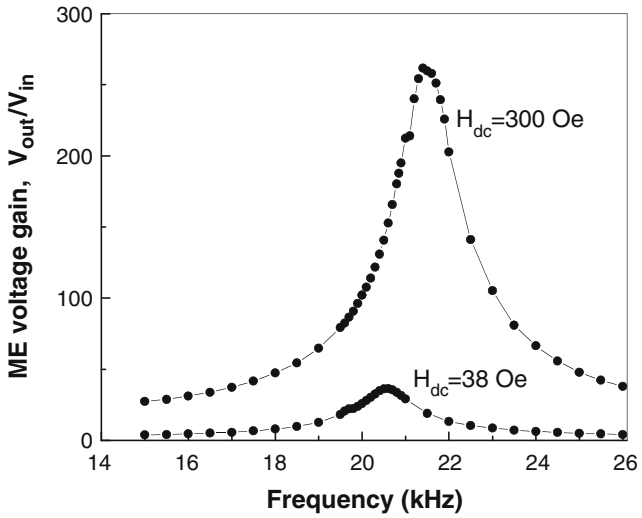


**Fig. 18** Voltage gain of ME transformer as a function of the drive frequency

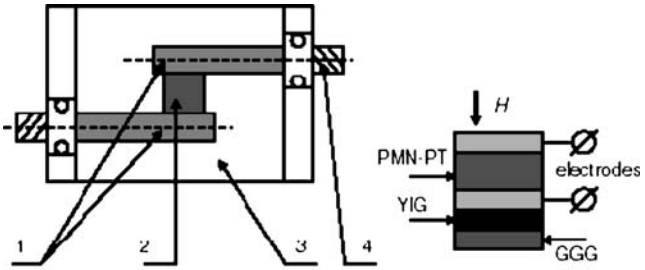


1: transmission lines, 2: ME resonator, 3: ground plane, 4: input/output

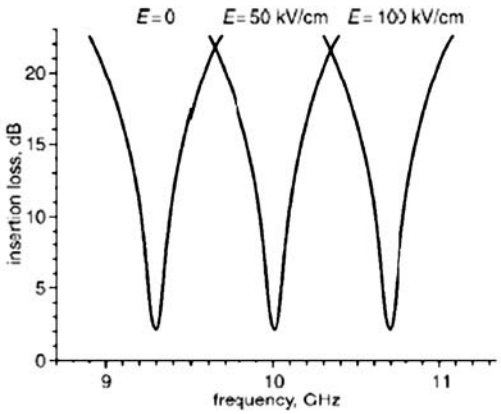


**Fig. 19** **a** Schematic diagram showing a microwave ME filter, and **b** Transmission characteristics for ME microwave filter (© 2005 IEEE, taken from [87]

induced voltage was strongly dependent on the operational frequency. When the current frequency was less than 100 Hz, the flux change rate passing through the coil was so small that the signal detected by the coil disappeared into the noise floor.

## 8.4 ME transformers

An extremely high voltage gain effect at resonant state has been reported in a long-type ME laminate consisting of magnetostrictive Terfenol-D and piezoelectric $Pb(Zr,Ti)O_3$ (PZT) layers [71]. A solenoid with N turns around the laminate that carries a current of $I_{in}$ was used to excite an ac magnetic field $H_{ac}$. The input ac voltage applied to the coils was $V_{in}$. When the frequency of $H_{ac}$ is equal to the resonance frequency of the laminate, the magnetoelectric coupling effect is sufficiently strong that the output ME voltage ($V_{out}$) induced in the piezoelectric layer is much higher than $V_{in}$. Thus, under resonant drive, our ME laminate exhibits a strong voltage gain, offering potential for high-voltage miniature transformer applications.

Figure 18 shows the measured voltage gain $V_{out}/V_{in}$ as a function of the drive frequency $f$ for a ME transformer with Terfenol-D layers of 40 mm in length and a piezoelectric layer of 80 mm in length. A maximum voltage gain of ~260 was found at a resonance frequency of 21.3 kHz. In addition, at the resonance state, the maximum voltage gain of the ME transformer was strongly dependent on an applied dc magnetic bias $H_{dc}$, which is due to the fact that Terfenol-D has a large effective piezomagnetic coefficient only under a suitable $H_{dc}$.

Compared with conventional electromagnetic transformers, our ME transformer does not require secondary coils with a high-turn ratio in order to obtain a step-up voltage output. Compared with piezoelectric transformers, it has significantly higher voltage gains and a notably wider bandwidth. Also, it has the additional advantage of low input impedance; thus requiring low-voltage current drive for the magnetostrictive Terfenol-D layers, and a high output impedance for the PZT one. Terfenol-D has a very high energy density of 4.9–25 $kJ/m^3$, which is notably higher than that of PZT used in conventional piezoelectric transformers. The combination of these advantages offers potential for applications in new solid-state transformer devices.

## 8.5 ME filter

An electric field tunable microwave band-pass filter based on ferromagnetic resonance (FMR) in a bilayer of yttrium iron garnet (YIG) and PMN-PT has been designed by Srinivasan et al [87]. The filter tunability is accomplished through magnetoelectric (ME) coupling that manifests as a shift in the FMR. The single-resonator filter consists of microstrip transmission lines of non-resonant length, a bilayer of YIG (GGG)/PMN–PT (GGG—gadolinium gallium garnet) and a metal plated dielectric ground plane as shown in Fig. 19a. Off-resonance input–output decoupling is determined by the gap between the transmission lines. Input–output coupling is realized when a bias magnetic field corresponding to FMR is present.

The estimated device results on insertion loss $L$ vs. frequency $f$ are shown in Fig. 19b. The results showed linear variation in the central frequency with electric field ($E$) and electric field tenability over a frequency band of 1.4 GHz. A tenability of 420 MHz was determined on application of $E$= 30 kV/cm. The filter was predicted to have a bandwidth of 80 MHz and total insertion loss as low as 2.5 dB.

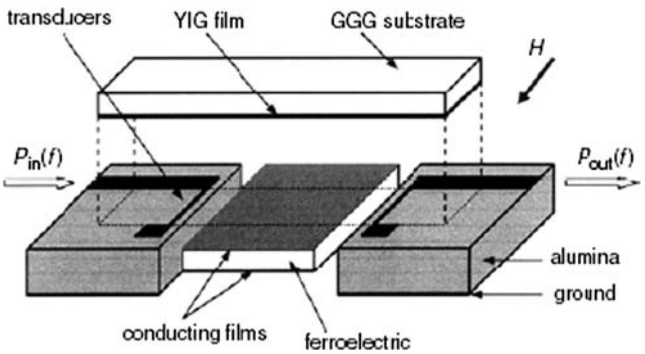


**Fig. 20** A magnetoelectric microwave phase shifter (© 2005 IEEE, taken from [88]

### 8.6 ME phase shifter

An electric field tunable YIG (GGG)-PZT phase shifter based on ferromagnetic resonance (FMR) has been designed and characterized by Srinivasan et al [88]. The piezoelectric deformation in PZT by applying an electric field E leads to a shift in the FMR frequency in YIG and a phase shift. The design for the magnetostatic wave (MSW) phase shifter is shown in Fig. 20 [88]. It consisted of a 4 mm×4 mm× 0.5 mm plate of PZT and a 2 mm×25 $mm^2$ epitaxial (111) YIG film of thickness 15 μm on gadolinium gallium garnet (GGG) substrate. Silver electrodes were deposited on PZT. A phase shift of +90° was obtained by applying an electric field of $E$=8 kV/cm across the PZT. When the direction of E was reversed, the phase shift also reversed sign to −90°.

## 9 Summary

This review article provides a survey of the developments in the area of magnetoelectric composites. The focus in the paper was on composites consisting of piezoelectric and magnetostrictive phases. Properties of the composites synthesized using several different techniques including directional solidification, sintering, controlled precipitation and lamination was discussed. Directional solidification such as Bridgman technique or floating zone method are complex processes involving tight control over the composition, cooling rate and temperatures. On the other hand, sintered composites are easier and cheaper to fabricate with several advantages such as freedom on the selection of the constituents, variation in the starting particle sizes of the constituents, freedom of the selection of the sintering temperature, and does not require the presence of eutectic or eutectoid transformation. In spite of these advantages sintered composites provide an inferior response, as compared to hot-pressing or unidirectional solidification. Controlled precipitation technique combines the advantages offered by unidirectional solidification and sintering. Results reported on ME composites synthesized using this technique have indicated an enhancement by 50% in the magnitude of the ME coefficient. It has been mentioned that the controlled precipitation route provides the ability to (1) synthesize bulk material with crystallographically aligned nanoscale interfaces, (2) synthesize material with high interfacial area, (3) thermally control the microstructure and as a result properties of the material, and (4) synthesize grain oriented materials.

Laminate composites consisting of relaxor based piezoelectric single crystals and giant magnetostrictive material Terfenol-D have been found to exhibit large magnitudes of the ME coefficient. The magnitude of the ME coefficient is higher in the longitudinal magnetization direction as compared to transversal direction. The reason for this enhancement has been associated to the larger piezomagnetic and magneoelastic coupling coefficients of Terfenol-D in the longitudinal direction as compared to those in transverse. Further, the magnitude of the ME coefficient shows dramatic enhancement at the electromechanical resonance frequency of the material.

Several applications including power harvesting, current transformers, phase shifters, magnetic field sensors, current sensors, and filter utilizing the magnetoelectric effect have been discussed. Representative data on these applications clearly demonstrates success in designing magnetoelectric based components, and as such offers them a promising future.

**Acknowledgement** The authors (S. Priya and R. A. Islam) would like to acknowledge the support from DOE and Texas Higher Education Coordinating Board through grant number's DE-FG02-06ER46288 and 003656-0010-2006 respectively.

## References

1. J. Van Suchetelene, Philips Res. Rep. **27**, 28–37 (1972)
2. G. Smolenskii, V.A. Ioffe, Colloque International du Magnetisme, Communication No. 71 (1958)
3. D.N. Astrov, B.I. Al'shin, R.V. Zhorin, L.A. Drobyshev, Sov. Phys. JETP **28**, 1123 (1968)
4. R.M. Hornreich, Solid State Commun. **7**, 1081–1085 (1969)
5. E. Fischer, G. Gorodetsky, R.M. Hornreich, Solid State Commun. **10**, 1127–1132 (1972)
6. T. Kimura, T. Goto, H. Shintani, K. Ishizaka, T. Arima, Y. Tokura, Nature **426**, 55–58 (2003)
7. T. Lottermoser, T. Lonkai, U. Amann, D. Hohlwein, J. Ihringer, M. Feibig, Nature **430**, 541–544 (2004)
8. M. Feibig, T. Lottermoser, D. Fröhlinch, A.V. Goltsev, R.V. Pisarev, Nature **419**, 818–820 (2002)
9. C. Ederer, N.A. Spaldin, Nature Mater **3**, 849–851 (2004)
10. N. Hur, S. Park, P.A. Sharma, J.S. Ahn, S. Guha, S.-W. Cheong, Nature **429**, 392–395 (2004)
11. B.B. Vanaken, T.T.M. Palstra, A. Filippetti, N. Spaldin, Nature Mater **3**, 164–170 (2004)
12. M. Fiebig, J. Phys. D, Appl. Phys. **38**, R123–R152 (2005)
13. H. Schmid, H. Reider, E. Ascher, Solid State Commun. **3**, 327 (1965)
14. S.V. Suryanarayana, Bull. Mater. Sci. **17**(7), 1259–1270 (1994)
15. R.S. Singh, Ph. D. Thesis, Osmania University, Hyderabad, India, (1996)
16. R.S. Singh, T. Bhimasankaram, G.S. Kumar, S.V. Suryanarayana, Solid State Commun. **91**, 567 (1994)
17. A. Srinivas, D.-W. Kim, K.S. Hong, S.V. Suryanarayana, Mater. Res. Bull. **39**, 55–61 (2004)
18. B. Ruette, S. Zvyagin, A. Pyatakov, A. Bush, J.F. Li, V. Belotelov, A. Zvezdin, D. Viehland, Phys. Rev., B. **69**, 064114 (2004)
19. A.M. Kadomtseva, A.K. Zvezdin, Y. Popov, A. Pyatakov, G. Vorob'ev, JETP Lett. **79**, 571 (2004)
20. J. Wang, J. Neaton, H. Zheng, V. Nagarajan, S. Ogale, B. Liu, D. Viehland, V. Vaithyanathan, D. Schlom, U. Waghamare, N. Spaldin, K. Rabe, M. Wuttig, R. Ramesh, Science **299**, 1719 (2003)
21. J.F. Li, J. Wang, N. Wang, B. Ruette, A. Pyatakov, M. Wuttig, R. Ramesh, A. Zvezdin, D. Viehland, Appl. Phys. Letters **84**, 5261 (2004)

22. M. Murakami, S. Fujino, S.-H. Lim, L.G. Salamanca-Riba, M. Wuttig, I. Takeuchi, B. Varughese, H. Sugaya, T. Hasegawa, S.E. Lofland, Appl. Phys. Lett. **88**, 112505 (2006)
23. X.Y. Zhang, C.W. Lai, X. Zhao, D.Y. Wang, J.Y. Dai, Appl. Phys. Lett. **87**, 143102 (2005)
24. J. van den Boomgaard, D.R. Terrell, R.A.J. Born, H.F.J.I. Giller, J. Mater. Sci. **9**, 1705–1709 (1974)
25. J. van den Boomgaard, R.A.J. Born, J. Mater. Sci. **13**, 1538–1548 (1978)
26. Y.R. Dai, P. Bao, J.S. Zhu, J.G. Wan, H.M. Shen, J.M. Liu, J. Appl. Phys. **96**(10), 5687–5690 (2004)
27. G. Srinivasan, C.P. DeVreugd, C.S. Flattery, V.M. Laletsin, N. Paddubnaya, Appl. Phys. Lett. **85**(13), 2550–2552 (2004)
28. S. Mazumder, G.S. Bhattacharya, Ceram. Int. **30**, 389–392 (2004)
29. L. Fuentes, M. GarcÍa, D. Bueno, M.E. Fuentes, A. Muñoz, Ferroelectrics **336**, 81–89 (2006)
30. T.G. Lupeiko, S.S. Lopatin, I.V. Lisnevskaya, B.I. Zvyagintsev, Inorg. Mater. **30**, 1353 (1994)
31. R.P. Mahajan, K.K. Patankar, M.B. Kothale, S.A. Patil, Bull. Mater. Sci. **23**(4), 273–279 (2000)
32. K.K. Patankar, S.A. Patil, K.V. Sivakumar, R.P. Mahajan, Y.D. Kolekar, M.B. Kothale, Mater. Chem. Phys. **65**, 97–102 (2000)
33. J. Ryu, S. Priya, K. Uchino, D. Viehland, H. Kim, J. Korean Ceram. Soc. **39**, 813–817 (2002)
34. M.I. Bichurin, D.A. Filippov, V.M. Petrov, V.M. Laletsin, N. Paddubnaya, G. Srinivasan, Phys. Rev. B **68**, 132408 (2003)
35. M.J. Dapino, F.T. Calkins, A.B. Flatau, in *22nd Encyclopedia of Electrical and Electronics Engineering*, vol. 12 (Wiley, 1999), pp. 278–305
36. A.E. Clark, in *Ferromagnetic Materials*, vol. 1, ed. by E.P. Wohlfarth (North Holland, Amsterdam, 1980), pp. 531–589
37. E. du Trémolet de Lacheisserie, *Magnetostriction Theory and Applications of Magnetoelasticity*, (CRC Press, Boca Raton, FL, 1993)
38. J.B. Restorff, in *Encyclopedia of Applied Physics*, vol. 9 (VCH, New York, 1994), pp. 229–244
39. J. Smit, H.P.J. Wijn, in *Ferrites*, vol. 169 (Philips Technical Library, Eindhoven, Netherlands, 1959), pp. 230–231
40. C.M. Srivastava, C. Srinivasan, *Science of Engineering Materials* (Wiley Eastern, New Delhi, 1987), pp. 301–348
41. APC International, *Piezoelectric Ceramics*, (Catalogue of Materials, Mackeyville, PA)
42. S. Park, T. Shrout, IEEE Trans. Ultrason. Ferroelect. Freq. Contr. **44**(5), 1140–1147 (1997)
43. T. Ikeda, *Fundamentals of Piezoelectricity* (Oxford University Press, New York, 1990)
44. *Landolt–Bornstein Series on Ferroelectric Oxides,* III/16a, (Springer-Verlag, Berlin Heidelberg, 1999)
45. R.P. Santoro, R.E. Newnham, Technical Report AFML TR-66-327, (Air Force Materials Lab, OH) 1966
46. A.V. Shubnikov, *Symmetry and Antisymmetry of Finite Figures* (USSR Academy of Sciences, Moscow, 1951)
47. R.R. Birss, *Symmetry, Magnetism* (North-Holland, Amsterdam, 1966)
48. R.E. Newnham, Ferroelectrics **68**, 1–32 (1986)
49. W.F. Brown Jr., R. Hornreich, S. Shtrikman, Phys. Rev. **168**, 574 (1968)
50. T.H. O'Dell, Phila. Mag. **8**, 411 (1963)
51. J. Echigoya, S. Hayashi, Y. Obi, J. Mater. Sci. **35**, 5587–5591 (2000)
52. W.E. Kramer, R.H. Hopkins, M.R. Daniel, J. Mater. Sci. **12**, 409–414 (1977)
53. J. Ryu, A.V. Carazo, K. Uchino, H.-E. Kim, J. Electroceram. **7**, 17 (2001)
54. J. Ryu, S. Priya, K. Uchino, J. Electroceram. **8**, 107–119 (2002)
55. M.I. Bichurin, D.A. Filippov, V.M. Petrov, V.M. Laletsin, N. Paddubnaya, G. Srinivasan, Phys. Rev. B **68**, 054402 (2003)
56. G. Srinivasan, E.T. Rasmussen, R. Hayes, Phys. Rev., B **67**(1), 014418 (2003)
57. G. Srinivasan, E. Rasmussen, B. Levin, R. Hayes, Phys. Rev., B **65**, 134402 (2002)
58. R.A. Islam, S. Priya, Jpn. J. Appl. Phys. **45**(5), L128–L131 (2006)
59. R. Islam, S. Priya, in *Proceedings of 30th International Cocoa Beach Conference and Exposition on Advanced Ceramics and Composites*, FL, Jan 21–26, 2006 (in press)
60. R. Islam, S. Priya, Int. Ferroelec. (2007, in press)
61. J. Ryu, A. Vazquez Carazo, K. Uchino, H. Kim, Jpn. J. Appl. Phys. **40**, 4948–4951 (2001)
62. U. Lalestin, N. Padubnaya, G. Srinivasan, CP. Devreugd, Appl. Phys., A Mater. Sci. Process. **78**(1), 33 (2004)
63. S.X. Dong, J. Zhai, J.-F. Li, D. Viehland, J. Appl. Phys. **88**, 082907 (2006)
64. S.X. Dong, J.F. Li, D. Viehland, IEEE Trans. Ultrason. Ferroelectr. Freq. Control **50**(10), 1253–1261 (2003)
65. S.X. Dong, J.F. Li, D. Viehland, J. Appl. Phys. **96**, 3382 (2004)
66. S.X. Dong, J. Cheng, J.F. Li, D. Viehland, Appl. Phys. Lett. **83**, 4812 (2003)
67. S.X. Dong, J.F. Li, D. Viehland, Appl. Phys. Lett. **85**, 5305 (2004)
68. S.X. Dong, Junyi Zhai, Zhengping Xing, J.F. Li, D. Viehland, Appl. Phys. Lett. **86**, 102901 (2005)
69. J. Zhai, Z. Xing, S.X. Dong, J.F. Li, D. Viehland, Appl. Phys. Lett. **88**, 062510 (2006)
70. S.X. Dong, J.F. Li, D. Viehland, Appl. Phys. Lett. **85**, 2307 (2004)
71. S.X. Dong, J.F. Li, D. Viehland, Appl. Phys. Lett. **84**, 4188 (2004), Appl. Phys. Lett. **85**, 3534 (2004)
72. S.X. Dong, J.F. Li, D. Viehland, IEEE Trans. Ultrason. Ferroelectr. Freq. Control **51**(7), 794–799 (2004)
73. S.X. Dong, J. Zhai, F. Bai, J.F. Li, D. Viehland, T.A. Lograsso, J. Appl. Phys. **97**, 103902 (2005)
74. S.X. Dong, J. Zhai, N. Wang, F. Bai, J.F. Li, D. Viehland, T.A. Lograsso, Appl. Phys. Lett. **87**, 222504 (2005)
75. S. Narendra Babu, T. Bhimasankaram, S.V. Suryanarayana, Bull. Mater. Sci. **28**(5), 419–422 (2005)
76. V.M. Laletin, N. Paddubnaya, G. Srinivasan, C.P. De Vreugd, M.I. Bichurin, V.M. Petrov, D.A. Filippov, Appl. Phys. Lett. **87**, 222507 (2005)
77. C. -W. Nan, L. Liu, N. Cai, J. Zhai, Y. Ye, Y.H. Lin, L J. Dong, C. X. Xiong, Appl. Phys. Lett. **81**, 3831 (2002)
78. N. Cai, J. Zhai, C.W. Nan, Y. Lin, Z. Shi, Phys. Rev. B **68**, 224103 (2003)
79. Z. Shi, C. -W. Nan, J. M. Liu, D.A. Filippov, M.I. Bichurin, Phys. Rev., B **70**, 134417 (2004)
80. S.X. Dong, J. Zhai, F. Bai, J.F. Li, D. Viehland, Appl. Phys. Lett. **87**, 052502 (2005)
81. S.X. Dong, J.F. Li, D. Viehland, IEEE Trans. Ultrason. Ferroelectr. Freq. Control **50**(10), 1236–1239 (2003)
82. S.X. Dong, J.-F. Li, D. Viehland, J. Mater. Sci. **41**, 97–106 (2006)
83. B.O'Handley, J.K. Huang, Enhanced Performance is Piezo-based Energy Harvesters. Presented at UTA Workshop on Piezoelectric Energy Harvesting, The University of Texas Arlington, TX, Jan. 27, 2006
84. M.D. Mermelstein, A. Dandrige, Appl. Phys. Lett. **51**(7), 545–547 (1987)
85. T. Ueno, T. Higuchi, IEEE Trans. Magn. **41**(10), 3670–3672 (2005)
86. E. Quandt, S. Stein, M. Wuttig, IEEE Trans. Magn. **41**(10), 3667–3669 (2005)
87. G. Srinivasan, A.S. Tatarenko, M.I. Bichurin, Electron. Lett. **41** (10), 596–598 (2005)
88. Y.K. Fetisov, G. Srinivasan, Electron. Lett. **41**(19), 1066–1067 (2005)